

Observational constraints of diffusive dark-fluid cosmology

Remudin Reshid Mekuria^{1a} and Amare Abebe^{2,3b}

¹ *Faculty of Engineering and Computer Science,*

Ala-too International University, Bishkek, Kyrgyzstan

² *Centre for Space Research, North-West University, Potchefstroom, South Africa and*

³ *National Institute for Theoretical and Computational Sciences (NITheCS), South Africa*

(Dated: January 10, 2023)

Abstract

In this work, we consider an interacting dark-fluid cosmological model in which energy exchange between dark matter and dark energy occurs through diffusion. After solving the background expansion history for a late-time universe, we attempt to constrain the cosmological parameters by comparing simulated values of the model against Supernovae Type 1A data. We consider four different cases and compare them against the Λ CDM model as the "true model". Our results show that the diffusive model in which dark energy flows to dark matter is the most likely alternative to Λ CDM model. This model is not only in line with Planck 2018 observational results but can also give a potential explanation to the so-called Hubble tension.

PACS numbers: 04.50.Kd, 98.80.Jk, 98.80.-k, 95.36.+x, 98.80.Cq

arXiv:2301.02913v1 [astro-ph.CO] 7 Jan 2023

^a Remudin.Mekuria@gmail.com

^b Amare.Abebe@nithecs.ac.za

I. INTRODUCTION

A lot has already been reported about the discrepancy between observational findings [1–6] and theoretical predictions of the expansion history of the universe in standard cosmology. The missing matter and energy in the universe, dubbed dark matter (DM) and dark energy (DE), respectively, account for a whopping 95% of the total content of the universe. The nature of these dark components of the universe is not properly understood, but there are several candidates in the literature, including unified dark-fluid models, proposed to describe them and their effect on astrophysics and cosmology. On the DM side, most commonly studied candidates include Weakly Interacting Massive Particles (WIMPS) [7–10] or some astrophysical modification of gravity such as the Modified Newtonian Dynamics (MOND)[11] among many others, whereas on the DE side, the cosmological constant Λ [12] is perhaps the simplest addition to the standard cosmological model needed to explain most of the observed data. There are some serious issues associated with the cosmological constant, however, such as the eponymous *cosmological constant problem* [13] and the coincidence problem [14, 15] which make the choice less attractive. That is why there are currently a plethora of other alternatives to explain current cosmological observations, such as modifications to the gravitational theory itself (see, for example, [16–19]), an evolving Λ [20–22], deviations from the standard homogeneous (see [23, 24] and references therein) and isotropic universe (such as the various Bianchi cosmological models) assumption, or some form of combination of these, among others.

Another aspect to consider, and one gaining much traction recently, is the interaction of dark matter and dark energy [3, 25–28]. Such an approach is interesting because it has the potential to explain the cosmological and coincidence problems, the Hubble tension and/or the σ_8 discrepancy [29–31].

Our current work pursues the last aspect, and studies the cosmological viability of a model [3] of the dark-fluid interaction using Supernovae Type 1A data. We organise the rest of the manuscript as follows: in Sec. II we give a covariant thermodynamics description of, and derive the field equations for, the background universe involving the diffusive dark-fluid system. In Sec. III we give an observational-constraint analysis using MCMC simulations of Supernovae Type 1A and Planck 2018 data and give some predictions on the values of the defining parameters of our model. Finally in Sec. IV we discuss the results and give conclusions.

II. BACKGROUND THERMODYNAMICS

The standard Λ CDM cosmology is a solution of the Einstein field equations (EFEs) derived from the action (From here onwards, we will work with units in which the speed of light $c = 1$):

$$S = \frac{c^4}{16\pi G} \int d^4x \sqrt{-g} [R + 2(L_m - \Lambda)] , \quad (1)$$

where R , L_m and Λ are the Ricci scalar, the matter Lagrangian density and the cosmological constant, respectively. The corresponding EFEs read:

$$G_{\mu\nu} + \Lambda g_{\mu\nu} = 8\pi G T_{\mu\nu} , \quad (2)$$

with the first (geometric) term represented by the Einstein tensor, and the RHS of the equation representing the total energy-momentum tensor (EMT) of matter fluid forms. Both $G_{\mu\nu}$ and $T_{\mu\nu}$ are covariantly conserved quantities. The EMT for perfect-fluid models is given by

$$T_{\mu\nu} = (\rho + p)u_\mu u_\nu + pg_{\mu\nu} , \quad (3)$$

where ρ and p are the energy density and isotropic pressure of matter, respectively, often related by the barotropic equation of state (EoS) $p = w\rho$ for a constant EoS parameter w . The normalised vector u_α represents the four-velocity of fundamental observers comoving with the fluid. The divergence-free EMT $T^{\mu\nu}{}_{;\mu} = 0$ leads to the fluid conservation equation

$$\dot{\rho} + 3\frac{\dot{a}}{a}(1+w)\rho = 0 , \quad (4)$$

where $a(t)$ is the cosmological scale factor whose evolution is given by the Friedmann equation

$$\frac{\dot{a}^2}{a^2} = \frac{8\pi G}{3}\rho + \frac{\Lambda}{3} - \frac{k}{a^2} \quad (5)$$

where k is the normalised spatial curvature parameter with values $-1, 0, 1$ depending on an open, flat or closed spatial geometry. In a multi-component fluid system, it is usually assumed that the energy density of each perfect-fluid component is assumed to evolve independently of the other fluids of the system:

$$\dot{\rho}_i + 3\frac{\dot{a}}{a}(1+w)\rho_i = 0 , \quad (6)$$

and in this case the EMT in Eq. (3) is the algebraic sum of the EMTs of each fluid, so are the total energy density and total pressure terms of Eq. (5) the algebraic sums of the individual components.

However, if we relax this assumption due to the presence of diffusion between the constituent components of the fluid, the individual components do not obey the matter conservation equation, but the total fluid still does. For the the i th component fluid, the new conservation equation reads:

$$T_i^{\mu\nu}{}_{;\mu} = N_i^\nu, \quad (7)$$

where N_i^ν corresponds to the current of diffusion term for that fluid. One can then write the non-conservation equation for the fluid as:

$$\dot{\rho}_i + 3\frac{\dot{a}}{a}(1+w)\rho_i = \frac{\gamma_i}{a^3}, \quad (8)$$

where γ_i is a constant for that fluid such that $\sum_i \gamma_i = 0$. Integrating this equation gives

$$\rho_i = a^{-3(1+w_i)} \left[\rho_{i0} + \gamma_i \int_{t_0}^t a^{3w_i} dt' \right], \quad (9)$$

with ρ_{i0} representing the present-day ($t = t_0$) value of the energy density of the i th fluid. Using a late-time $t - t_0 \ll t_0$ expansion and expressing $a(t) = a_0 [1 - (t_0 - t)H_0 + \dots]$, we can write the last term of the above integrand as

$$\begin{aligned} \int_{t_0}^t a^{3w_i} dt &= \int_{t_0}^t a^{3w_i} [1 - (t_0 - t)H_0 + \dots]^{3w_i} dt' \\ &= -\frac{1}{1+3w_i} [(1 + (t_0 - t)H_0)^{1+3w_i} - (1 + (t_0 - t)H_0)^{1+3w_i} + \dots] \\ &\approx \frac{1}{1+3w_i} [1 - (1 + (t_0 - t)H_0)^{1+3w_i}] \\ &= \frac{1}{(1+3w_i)H_0} [1 - (2 - a)^{1+3w_i}], \end{aligned} \quad (10)$$

where in the last step, we have used normalised the scale factor to unity today: $a_0 = 1$. Thus the energy density of each diffusive fluid component is given according to the below relation:

$$\rho_i = a^{-3(1+w_i)} \left[\rho_{i0} + \frac{\gamma_i}{(1+3w_i)H_0} [1 - (2 - a)^{1+3w_i}] \right]. \quad (11)$$

Assuming the well-known component of radiation, dust-like matter (baryons and dark matter) and vacuum energy, the above diffusive solution leads to:

$$\begin{aligned} \rho_r &= a^{-4} \left[\rho_{r0} + \frac{\gamma_r}{2H_0} [1 - (2 - a)^2] \right] \\ \rho_m &= a^{-3} \left[\rho_{m0} + \frac{\gamma_m}{H_0} [1 - (2 - a)] \right] \\ \rho_\Lambda &= \rho_{\Lambda 0} - \frac{\gamma_\Lambda}{2H_0} [1 - (2 - a)^{-2}] \end{aligned} \quad (12)$$

Let us now consider the Friedmann equation for the Λ CDM model, assuming $k = 0$, which can be given as:

$$\frac{\dot{a}^2}{a^2} = \frac{8\pi G}{3} \left[\rho_{r0} a^{-4} + \rho_{m0} + \frac{\gamma_m}{H_0} [1 - (2 - a)] a^{-3} + \rho_{\Lambda 0} - \frac{\gamma_\Lambda}{2H_0} [1 - (2 - a)^{-2}] \right]. \quad (13)$$

We are going to assume the diffusive interaction is limited between dark matter and dark energy for this work, and hence $\gamma_r = 0$ in the above equation.

Let us now introduce the following dimensionless quantities:

$$\Omega_i \equiv \frac{8\pi G}{3H_0^2} \rho_i, \quad \Delta_m \equiv \frac{8\pi G}{3H_0^3} \gamma_m, \quad \Delta_\Lambda \equiv \frac{8\pi G}{3H_0^3} \gamma_\Lambda, \quad 1 + z \equiv a^{-1}, \quad h \equiv \frac{H}{H_0}. \quad (14)$$

We can then show that the Friedmann equation can be recast as

$$h^2 = \Omega_{r0}(1+z)^4 + \Omega_{m0}(1+z)^3 + \Omega_{\Lambda 0} - \Delta_m z(1+z)^2 - \Delta_\Lambda \left[\frac{1}{2} - \frac{1}{2} \left(\frac{1+2z}{1+z} \right)^{-2} \right]. \quad (15)$$

Moreover, the deceleration parameter can be shown to be

$$q \equiv -\frac{\ddot{a}a}{\dot{a}^2} = \frac{4\pi G}{3H^2} \sum_i \rho_i (1 + 3w_i) = \frac{1}{2} \left\{ \frac{2\Omega_{r0}(1+z)^4 + \Omega_{m0}(1+z)^3 - 2\Omega_{\Lambda 0} - \Delta_m z(1+z)^2 + \Delta_\Lambda \left[1 - \left(\frac{1+2z}{1+z} \right)^{-2} \right]}{\Omega_{r0}(1+z)^4 + \Omega_{m0}(1+z)^3 + \Omega_{\Lambda 0} - \Delta_m z(1+z)^2 - \Delta_\Lambda \left[\frac{1}{2} - \frac{1}{2} \left(\frac{1+2z}{1+z} \right)^{-2} \right]} \right\} \quad (16)$$

These equations reduce to their respective Λ CDM limits when Δ_m and Δ_Λ both vanish.

III. OBSERVATIONAL CONSTRAINTS

In the following we will provide the result for observational constraints for the diffused dark fluid models we have introduced in this work. We have used the distance modulus equation which can be obtained by combining the different cosmological distance definitions to fit against the supernovae data in our MCMC simulation, which is presented in the work of [32].

As shown in Fig. 1 we run MCMC simulation for the diffusive model, by combining Eqs. 14 and 15, we find on average the best-fitting parameter value for each free parameter to be $h = 0.6966$ for the Hubble uncertainty parameter, $\Omega_{m0} = 0.2678$ for the matter density parameter, and $\Omega_{r0} = 0.00050$ for the radiation density parameter, along with a newly introduced parameters $\Delta_m = 0.00252$ and $\Delta_\Lambda = -0.00251$. We shall henceforth refer to this diffusive model case as Case I.

Among some of our optimum results we have also, as Case II, obtained the situation where Ω_{m0} result is much closer to the observational result of Planck 2018 ($= 0.315_{-0.111}^{+0.555}$) as shown below which

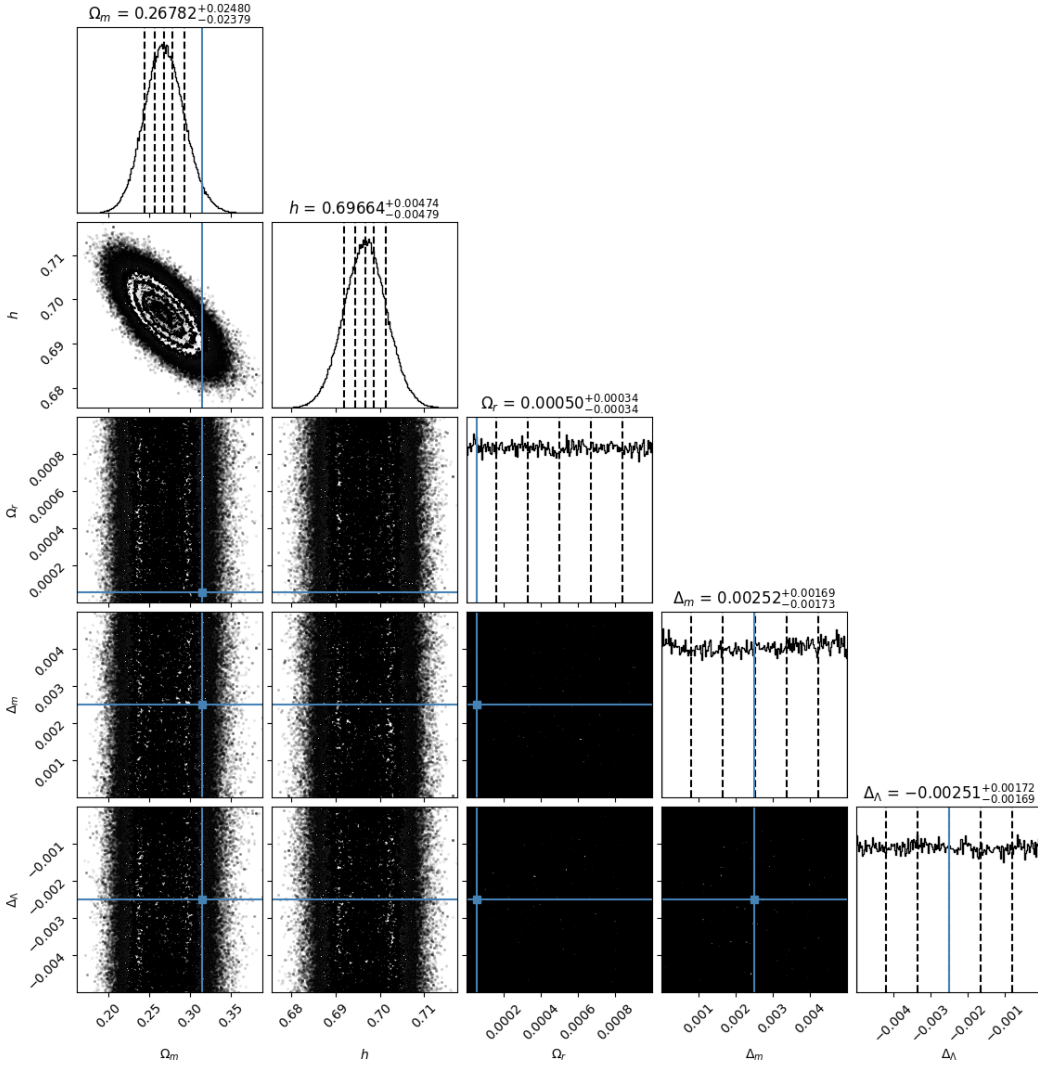


FIG. 1. The MCMC simulation results for the diffusive model's which is given in Eq. 15 for cosmological free parameters (Ω_{m0} , \bar{h} , Ω_{r0} , Δ_m and Δ_Λ), with the “true” values for $\Omega_{m0} = 0.315$, $\bar{h} = 0.674$, and $\Omega_{r0} = 2.47 \times 10^{-5} / \bar{h}^2$ provided by the Planck2018 collaboration data release [33]. We used 100 random walkers and 10000 iterations.

are also obtained with MCMC simulation for the diffusive model, by combining Eqs. 14 and 15, we find on average the best-fitting parameter value for each free parameter to be $h = 0.6955$ for the Hubble uncertainty parameter, $\Omega_{m0} = 0.3134$ for the matter density parameter, and $\Omega_{r0} = 0.00050$ for the radiation density parameter, along with a newly introduced parameters $\Delta_m = 0.1246$ and $\Delta_\Lambda = -0.1244$.

In Figs. 3 and 4 the above discussed two diffusive cosmological cases were given which clearly show to fit the extremely well with the data. Even the corresponding 1σ -deviation do not really have

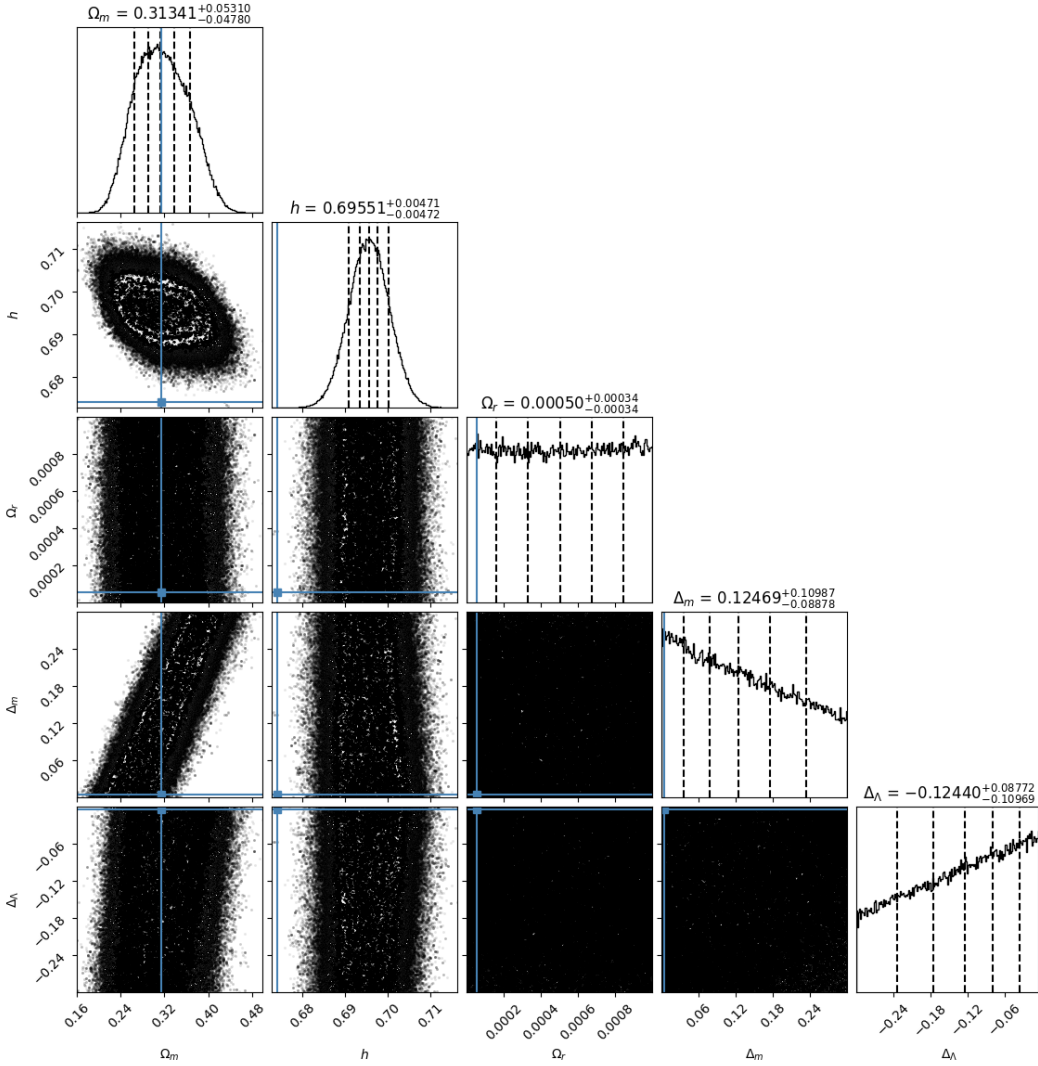


FIG. 2. The MCMC simulation results for the diffusive model's which is given in Eq. 15 for cosmological free parameters (Ω_{m0} , \bar{h} , Ω_{r0} , Δ_m and Δ_Λ), with the “true” values for $\Omega_{m0} = 0.315$, $\bar{h} = 0.674$, and $\Omega_{r0} = 2.47 \times 10^{-5} / \bar{h}^2$ provided by the Planck2018 collaboration data release [33]. We used 100 random walkers and 10000 iterations.

an impact on the full range predicted by them. Additionally, Figs. 5 and 6 display the residuals obtained in the above two cases. It can clearly be seen that at no point do the models over-or under-estimate the resulting distance modulus for each supernovae. We also note that the average off-set the model has, compared to the data, is $\bar{x}_{res} = -0.0374$ Mpc in both cases with a standard deviation of $\sigma_{res} = 0.2148$ and $\sigma_{res} = 0.2152$, respectively. These results show that these are very strong relationships between the models and the data points.

Figs. 7 and 8 shows the evolution of the Hubble parameter across the Redshift for two cosmological

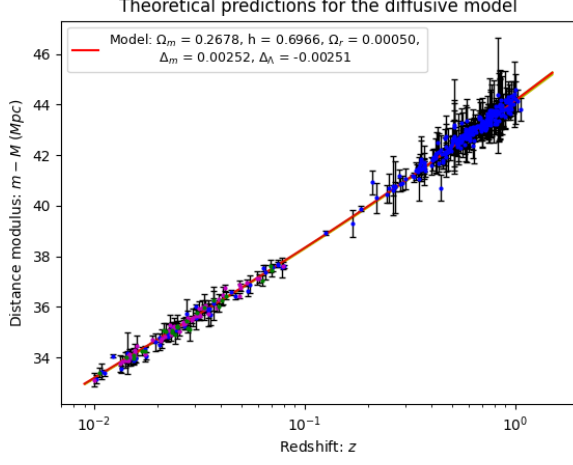


FIG. 3. The diffusive model's Eq. 15 for best-fitting free parameters for the Supernovae Type 1A data with cosmological parameter values as $h = 0.6966^{+0.0047}_{-0.0047}$, $\Omega_{m0} = 0.2678^{+0.0248}_{-0.0237}$, $\Omega_{r0} = 0.0005^{+0.0003}_{-0.0003}$, $\Delta_m = 0.0025^{+0.0169}_{-0.0173}$ and $\Delta_\Lambda = -0.0025^{+0.0172}_{-0.0169}$ of the MCMC simulation result shown in Fig. 1.

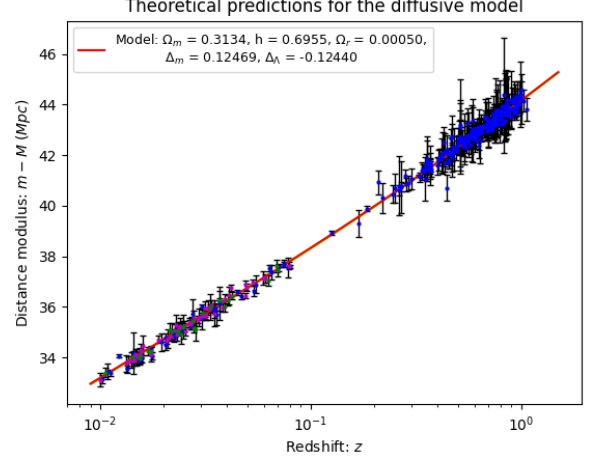


FIG. 4. The diffusive model's Eq. 15 for best-fitting free parameters for the Supernovae Type 1A data with cosmological parameter values as $h = 0.6955^{+0.0047}_{-0.0047}$, $\Omega_{m0} = 0.3134^{+0.0531}_{-0.0478}$, $\Omega_{r0} = 0.0005^{+0.0003}_{-0.0003}$, $\Delta_m = 0.1246^{+0.1098}_{-0.0887}$ and $\Delta_\Lambda = -0.1244^{+0.0877}_{-0.1096}$ of the MCMC simulation result shown in Fig. 2.

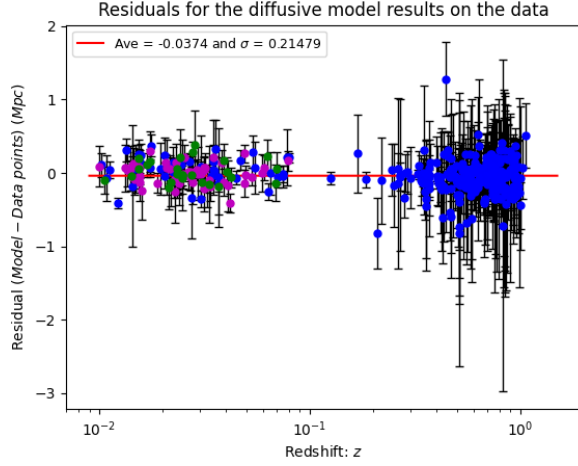


FIG. 5. This is the residuals distance in Mpc between the predicted model values and the data points for the diffusive model's Eq. 15 for best-fitting free parameters shown in Fig. 3.

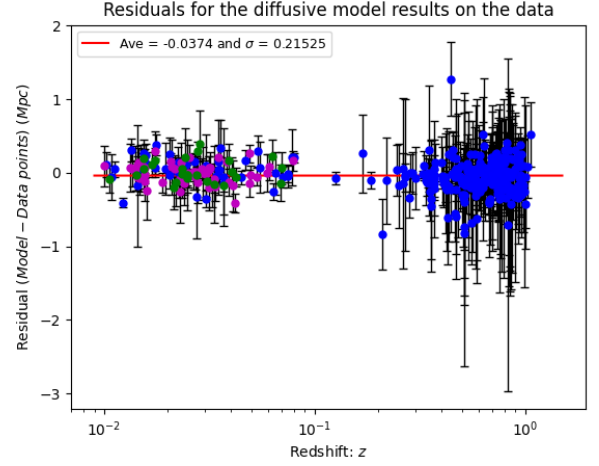


FIG. 6. This is the residuals distance in Mpc between the predicted model values and the data points for the diffusive model's Eq. 15 for best-fitting free parameters shown in Fig. 4.

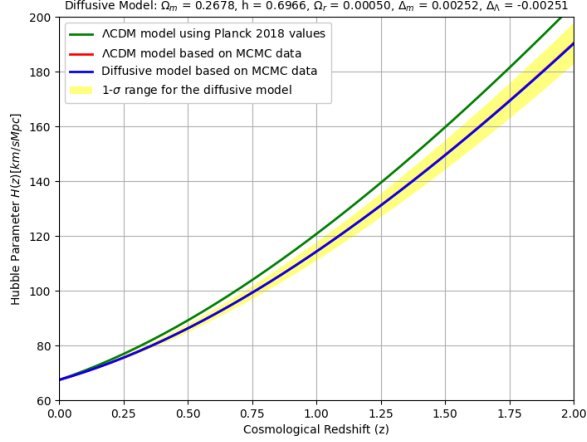


FIG. 7. The Hubble parameter vs Redshift for the Model displayed in Fig. 1. The blue curve represent the result obtained by considering diffusive fluid and employing MCMC simulation, with $1-\sigma$ deviation result displayed in yellowish shaded region. The red curve represent Λ CDM cosmology result using MCMC simulation where as the green curve represent one obtained directly by using the Planck 2018 data for the purpose of comparison.

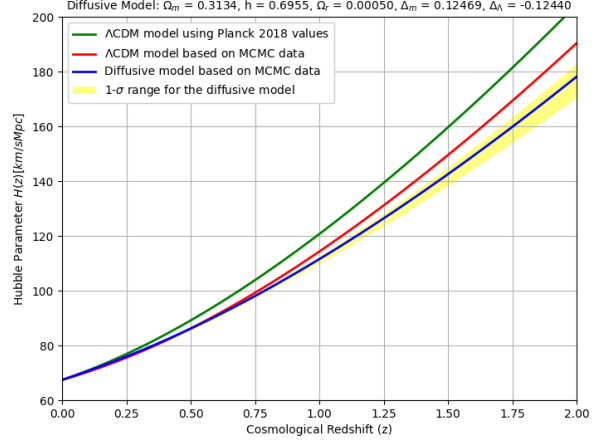


FIG. 8. The Hubble parameter vs Redshift for the Model displayed in Fig. 2. The blue curve represent the result obtained by considering diffusive fluid and employing MCMC simulation, with $1-\sigma$ deviation result displayed in yellowish shaded region. The red curve represent Λ CDM cosmology result using MCMC simulation where as the green curve represent one obtained directly by using the Planck 2018 data for the purpose of comparison.

model cases discussed above. The blue curves represent the results obtained by considering diffusive fluid and employing MCMC simulations, with $1-\sigma$ deviation results displayed in yellowish shaded regions. The red curves represent Λ CDM cosmology result using the average values obtained from the MCMC simulations where as the green curves represent those which are obtained directly by using the Planck 2018 data. In Fig. 7 a complete overlap is observed between the two curves which are obtained by using the MCMC simulation data in the Λ CDM model and the average value of MCMC simulation data in diffusive model. In contrast in the results of Fig. 8 we begin to notice a deviation between the two curves from $\sim z$ of 0.75 onward. Even though it is not expected to have a complete overlap between the Λ CDM model using Planck 2018 values put directly in the cosmological equations (green curves) and the MCMC results (blue curves and yellowish shaded regions), the difference between them is observed to be more prominent in the case of Fig. 8 than that of Fig. 7.

Fig. 9 and 10 shows the evolution of deceleration parameter across Redshift for the two diffu-

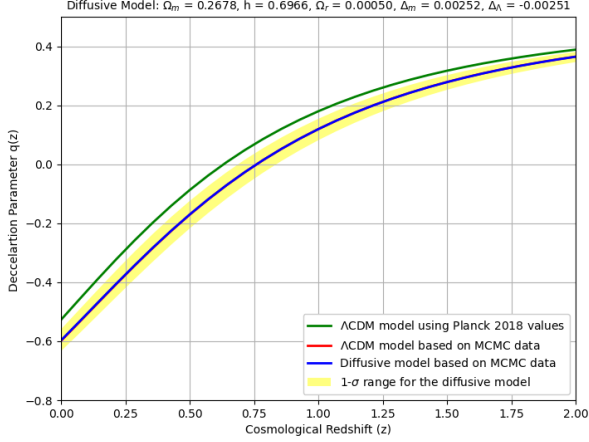


FIG. 9. The graph of deceleration parameter vs redshift for the diffusive model shown in Fig. 7.

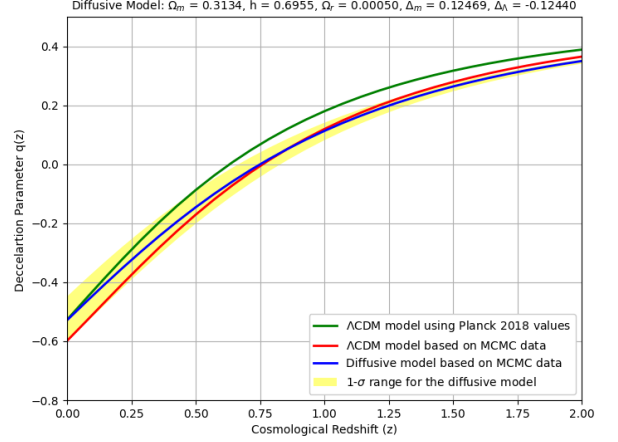


FIG. 10. The graph of deceleration parameter vs redshift for the diffusive model shown in Fig. 8.

sive cosmological model cases discussed above. The blue curves represent the results obtained by considering diffusive fluid and employing MCMC simulations, with $1-\sigma$ deviation results displayed in yellowish shaded regions. The red curves represent Λ CDM cosmological results by using the MCMC simulation data, where as the green curves represent those which are obtained directly by substituting the Planck 2018 data values. In Fig. 9 we observe a complete overlap between the two curves which are obtained by using MCMC simulation data in the Λ CDM equation and the average value of MCMC simulation data of the diffusive model, which is also observed in the Hubble parameter vs Redshift plot of Fig. 7. Moreover, the $1-\sigma$ deviation result which is indicated in the yellowish colored shaded region is observed to encompass all the curves for about ($z \sim 0.5$) of the deceleration parameter values given in Fig. 10. The diffusive model in this case has slightly larger values of deceleration parameter in the present universe ($z \sim 0$) compared to what is observed in the case of Fig. 9.

The above two cases (Case I and Case II) were obtained with a positive Δ_m and negative Δ_Λ . In what follows, let us provide the results corresponding to the cases of negative Δ_m which can be explained as being the situation when energy flows from dark matter sector to that of dark energy. As shown in Fig. 11 we run MCMC simulation for the diffusive model, by combining Eqs. 14 and 15, we find on average the best-fitting parameter value for each free parameter to be $h = 0.6967$ for the Hubble uncertainty parameter, $\Omega_{m0} = 0.2655$ for the matter density parameter, $\Omega_{r0} = 0.00050$ for the radiation density parameter, along with a newly introduced parameters $\Delta_m = -0.00251$ and $\Delta_\Lambda = 0.00246$. We will call this diffusive model case hereafter Case III.

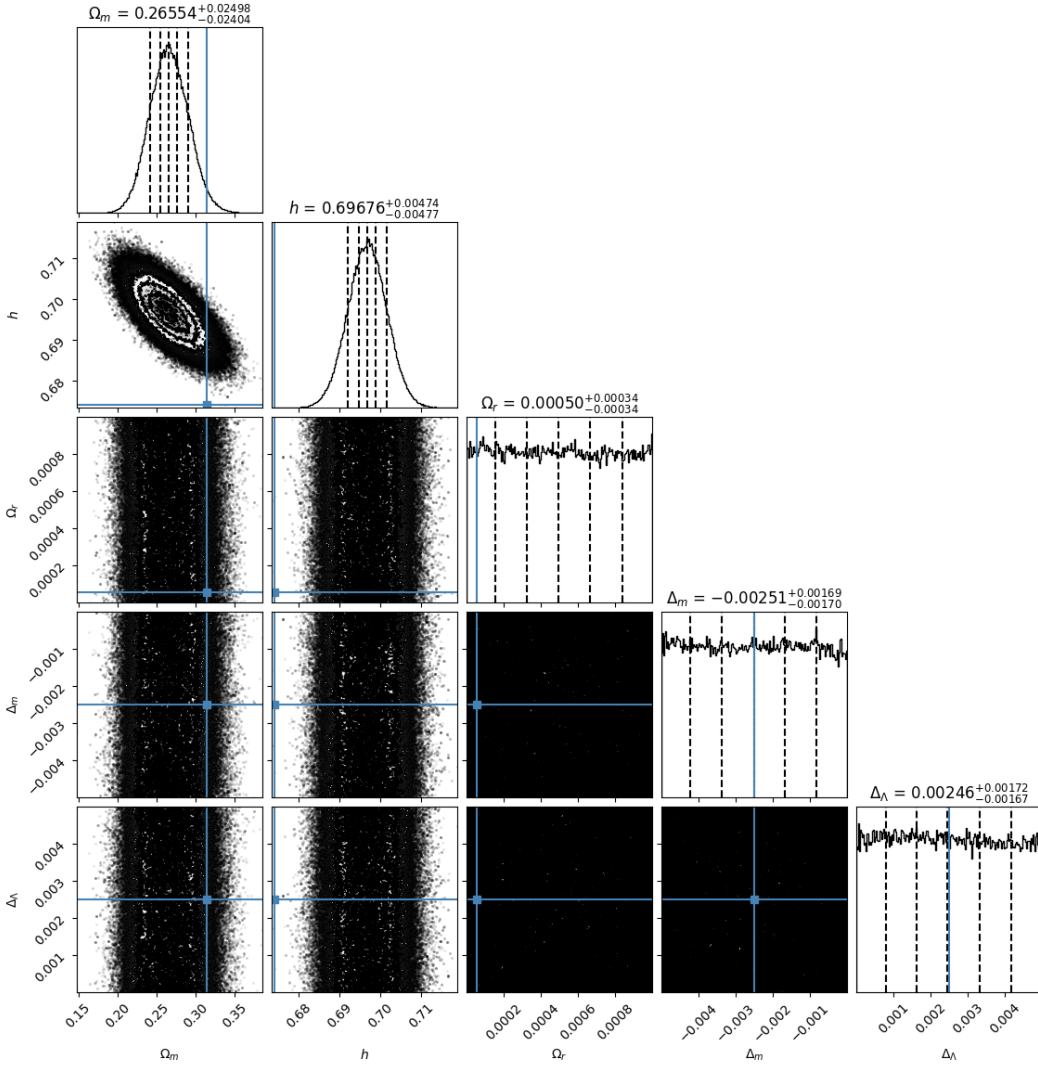


FIG. 11. The MCMC simulation results for the diffusive model's which is given in Eq. 15 for cosmological free parameters (Ω_{m0} , \bar{h} , Ω_{r0} , Δ_m and Δ_Λ), with the “true” values for $\Omega_{m0} = 0.315$, $\bar{h} = 0.674$, and $\Omega_{r0} = 2.47 \times 10^{-5} / \bar{h}^2$ provided by the Planck2018 collaboration data release [33]. We used 100 random walkers and 10000 iterations.

In the following we will also provide one interesting case in which the best-fitting parameter value for each free parameter to be $h = 0.6976$ for the Hubble uncertainty parameter, $\Omega_{m0} = 0.2283$ for the matter density parameter, and $\Omega_{r0} = 0.00050$ for the radiation density parameter, along with a newly introduced parameters $\Delta_m = -0.10747$ and $\Delta_\Lambda = 0.10426$. We will refer to this diffusive model case as Case IV.

In Fig. 13 and Fig. 14 the above discussed two diffusive cosmological model cases were given which clearly shows to fit the extremely well with the data. Even the corresponding 1σ -deviation do

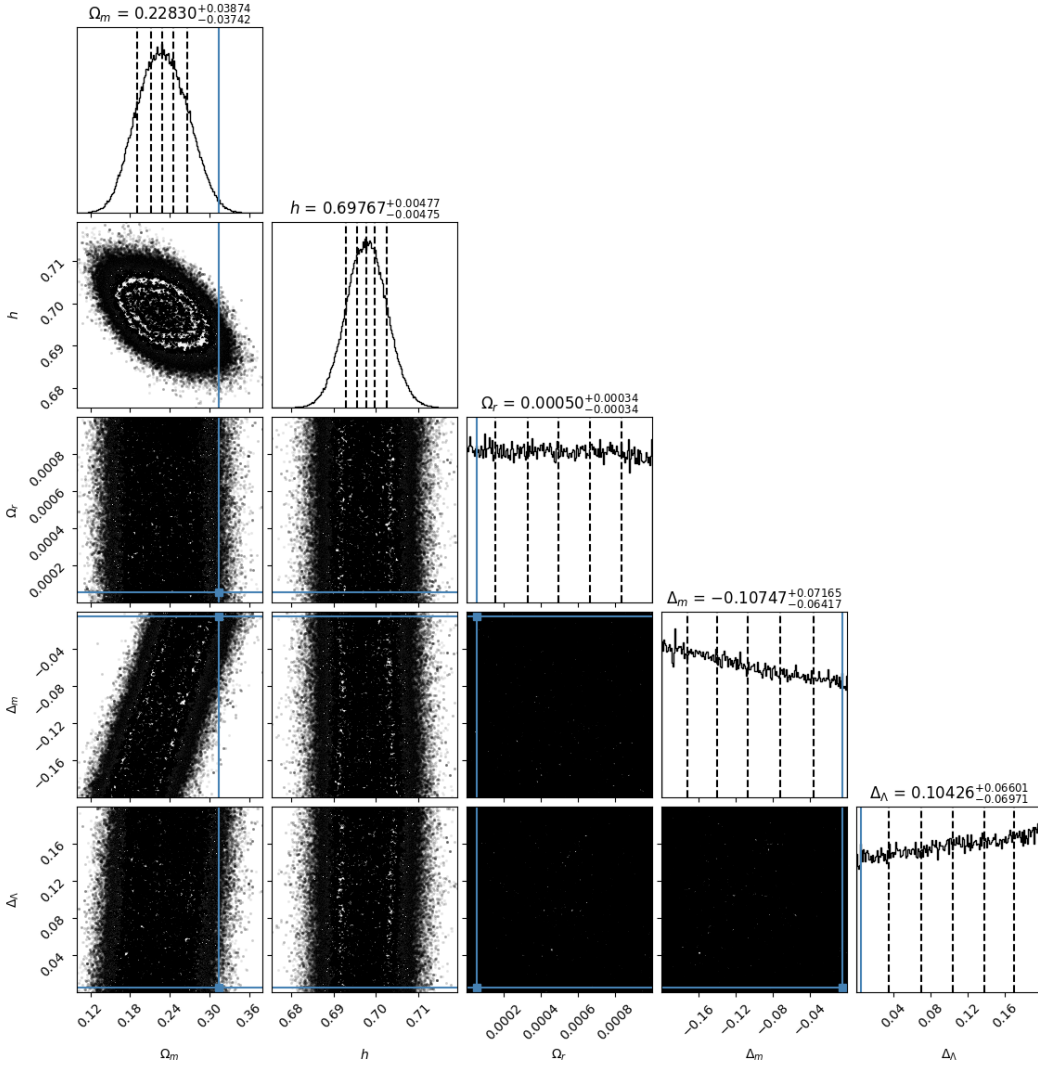


FIG. 12. The MCMC simulation results for the diffusive model's which is given in Eq. 15 for cosmological free parameters (Ω_{m0} , \bar{h} , Ω_{r0} , Δ_m and Δ_Λ), with the “true” values for $\Omega_{m0} = 0.315$, $\bar{h} = 0.674$, and $\Omega_{r0} = 2.47 \times 10^{-5} / \bar{h}^2$ provided by the Planck2018 collaboration data release [33]. We used 100 random walkers and 10000 iterations.

not really have an impact on the full range predicted by them.

Additionally, Fig. 15 and Fig. 16 displays the residuals obtained in the above two cases. It can clear be seen that at no point does the models over-or under-estimate the resulting distance modulus for each supernovae. We also note that the average off-set the model has, compared to the data, is $\bar{x}_{res} = -0.0374$ Mpc and $\bar{x}_{res} = -0.0386$ Mpc, with a standard deviation of $\sigma_{res} = 0.2147$ and $\sigma_{res} = 0.2145$, respectively. These results show that these are very strong relationships between the models and data points.

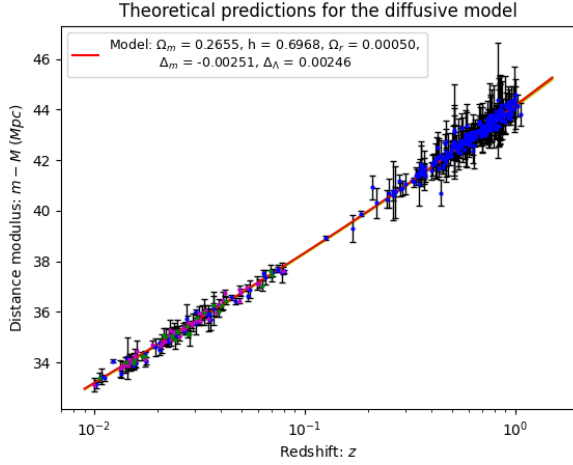


FIG. 13. The diffusive model's Eq. 15 for best-fitting free parameters for the Supernovae Type 1A data with cosmological parameter values as $h = 0.6967^{+0.0047}_{-0.0047}$, $\Omega_{m0} = 0.2655^{+0.0248}_{-0.0237}$, $\Omega_{r0} = 0.0005^{+0.0003}_{-0.0003}$, $\Delta_m = -0.0025^{+0.0169}_{-0.0170}$ and $\Delta_\Lambda = 0.0024^{+0.0172}_{-0.0167}$ of the MCMC simulation result shown in Fig. 11.

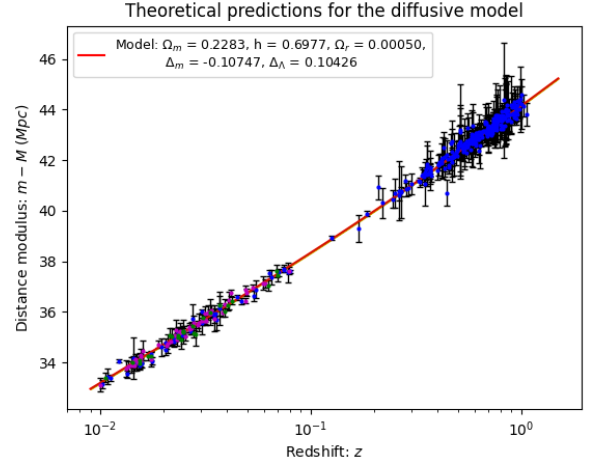


FIG. 14. The diffusive model's Eq. 15 for best-fitting free parameters for the Supernovae Type 1A data with cosmological parameter values as $h = 0.6976^{+0.0047}_{-0.0047}$, $\Omega_{m0} = 0.2283^{+0.0387}_{-0.0374}$, $\Omega_{r0} = 0.0005^{+0.0003}_{-0.0003}$, $\Delta_m = -0.1074^{+0.0716}_{-0.0641}$ and $\Delta_\Lambda = 0.1042^{+0.0660}_{-0.0697}$ of the MCMC simulation result shown in Fig. 12.

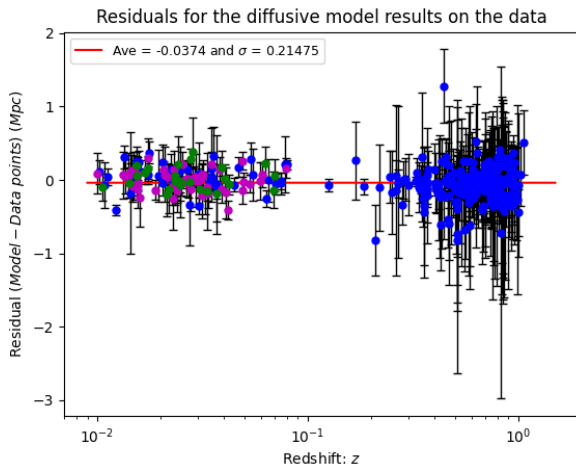


FIG. 15. This is the residuals distance in Mpc between the predicted model values and the data points for the diffusive model's Eq. 15 for best-fitting free parameters shown in Fig. 13.

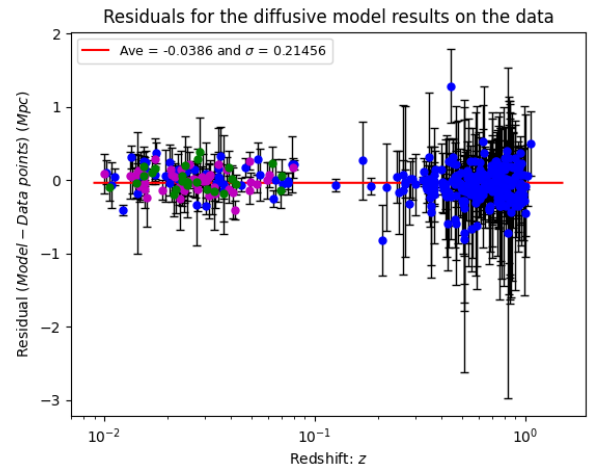


FIG. 16. This is the residuals distance in Mpc between the predicted model values and the data points for the diffusive model's Eq. 15 for best-fitting free parameters shown in Fig. 14.

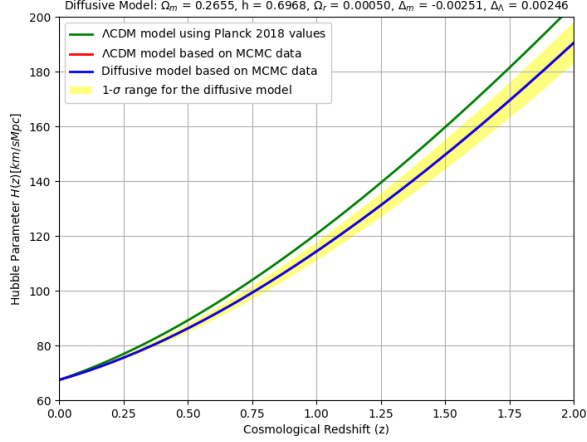


FIG. 17. The Hubble parameter vs Redshift for the Model displayed in Fig. 1. The blue curve represent the result obtained by considering diffusive fluid and employing MCMC simulation, with $1-\sigma$ deviation result displayed in yellowish shaded region. The red curve represent Λ CDM cosmology result using MCMC simulation where as the green curve represent one obtained directly by using the Planck 2018 data for the purpose of comparison.

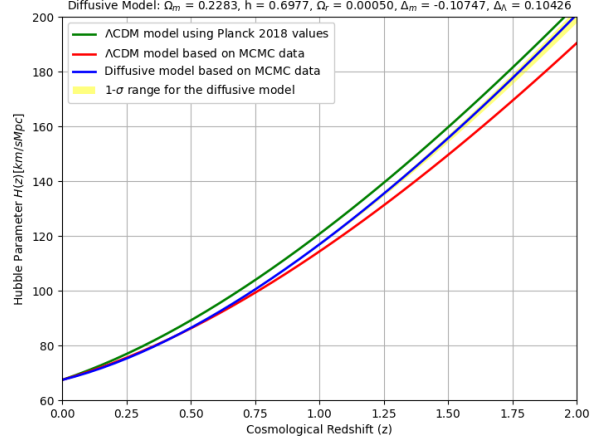


FIG. 18. The Hubble parameter vs Redshift for the Model displayed in Fig. 2. The blue curve represent the result obtained by considering diffusive fluid and employing MCMC simulation, with $1-\sigma$ deviation result displayed in yellowish shaded region. The red curve represent Λ CDM cosmology result using MCMC simulation where as the green curve represent one obtained directly by using the Planck 2018 data for the purpose of comparison.

Fig. 17 and 18 shows the evolution of the Hubble parameter across the Redshift for the two cosmological model cases discussed above. The blue curves represent the result obtained by considering diffusive fluid and employing MCMC simulation, with $1-\sigma$ deviation results displayed in yellowish shaded regions. The red curves represent Λ CDM cosmology result using MCMC simulation where as the green curves represent those obtained directly by using the Planck 2018 data. An overlap is observed in the result displayed in Fig. 17 between the two curves which are obtained by using the MCMC simulation data in the Λ CDM model and that of the average value of MCMC simulation data of the diffusive model. In contrast, a noticeable deviation emerges to be observed between the the Hubble parameter values of the diffusive model result (the blue curve) and that of the Λ CDM result based on MCMC simulation data (the red curve) in Fig. 18 from $\sim z$ of 0.75 onward. Even though it is not expected to have a complete overlap between the Λ CDM model using Planck 2018 values put directly in the cosmological equations (green curves) and the MCMC results (blue curves and yellowish shaded regions), the difference between them is observed to be more prominent in the

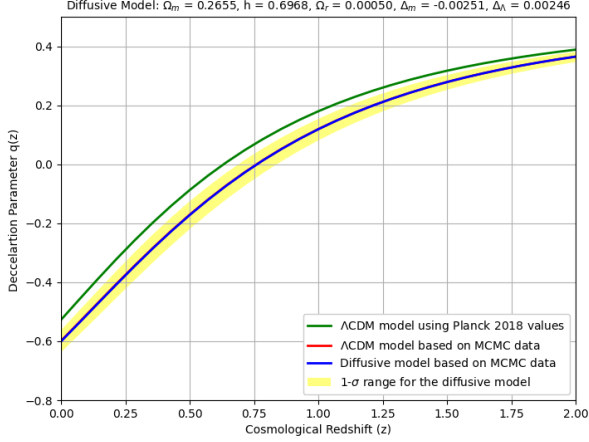


FIG. 19. The graph of deceleration parameter vs redshift for the diffusive model shown in Fig. 17.

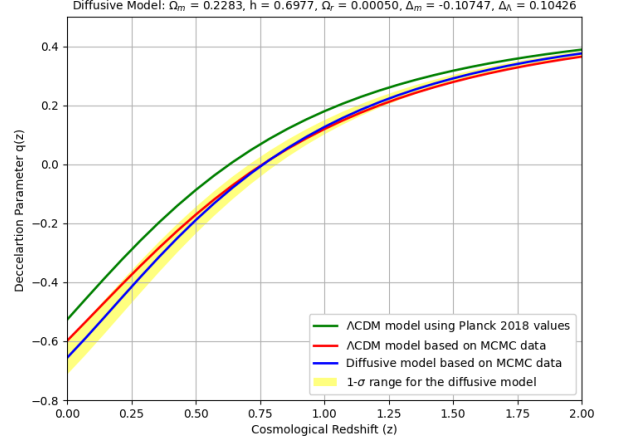


FIG. 20. The graph of deceleration parameter vs redshift for the diffusive model shown in Fig. 18.

case of Fig. 17 than that of Fig. 18.

Fig. 19 and 20 shows the evolution of the deceleration parameter across Redshift for the two cosmological model cases discussed above. The blue curves represent the result obtained by considering diffusive fluid and employing MCMC simulation, with $1-\sigma$ deviation results displayed in yellowish shaded regions. The red curves represent Λ CDM cosmology result using MCMC simulation where as the green curves represent those obtained directly by using the Planck 2018 data. In Fig. 19 we observe a complete overlap while using MCMC simulation data in the Λ CDM model and the average value of MCMC simulation data of the diffusive model, which is also observed in the Hubble parameter vs Redshift plot of Fig. 17.

As redshift increases, the Hubble parameter values of the diffusive model result (the blue curve) and that of the Λ CDM result based on MCMC simulation data (the red curve), begin to acquire similar values as can be seen in Fig. 20. The $1-\sigma$ deviation results indicated in yellow colored shaded region is observed to encompass both diffusive (blue curve) and non-diffusive (red curve) cases of the deceleration parameter values given in Fig. 20. In the current universe, the diffusive model has slightly lower values of deceleration parameter compared to what is observed in the case of Fig. 19.

In Table I we provide some statistical result which allows us to determine the best diffusive model case in comparisons to the Λ CDM model. The statistical analysis test that we have used is the Akaike information criterion (AIC) and Bayesian/Schwarz information criterion (BIC) selections which were used in a similar work in [32]. These information criteria evaluate the plausibility of an alternative model explaining the data compared to an “accepted/true model”. In our case the Λ CDM model will

TABLE I. The best-fit for each tested model, including the Λ CDM model. The models are listed in the order from the largest likelihood function value $\mathbf{L}(\hat{\theta}|\text{data})$ to the smallest likelihood of being viable. The reduced χ^2 -values are given as an indication of the goodness of fit for a particular model. The AIC and BIC values are shown, as well as the Δ AIC and Δ BIC for each information criterion. The Λ CDM model is chosen as the "true model".

Models	Δ_m	Δ_Λ	$\mathbf{L}(\hat{\theta} \text{data})$	χ^2	Red. χ^2	<i>AIC</i>	$ \Delta AIC $	<i>BIC</i>	$ \Delta BIC $
Diffusive Case II	+ve	-ve	-121.1677	242.3355	0.6845	252.3355	4.9405	271.7521	12.7072
Diffusive Case I	+ve	-ve	-120.7059	241.4118	0.6819	251.4118	4.0168	270.8285	11.7835
Λ CDM	0	0	-120.6975	241.3950	0.6780	247.3950	0	259.0449	0
Diffusive Case III	-ve	+ve	-120.6890	241.3781	0.6818	251.3781	3.9831	270.7947	11.7497
Diffusive Case IV	-ve	+ve	-120.3936	240.7872	0.6801	250.7872	3.3922	270.2039	11.1589

be considered as the "true model". Following the suggestion made in [32] as the calculated values for the AIC and BIC can be very random, we will also use the difference in AIC (i.e., Δ AIC) and BIC (i.e., Δ BIC) values of each model compared to the "true model's AIC and BIC values, and we use the Jeffrey's scale in order to make conclusions about the viability of the various Diffusive model cases. Moreover, the reduced χ^2 -values are used as an indication of the goodness of fit for each model on the supernovae data. It is observed that, the first two Diffusive model cases (shown in Fig. 1 and 2) have obtained better likelihood function values than the Λ CDM model based on a Gaussian probability distribution, with Case II obtaining the larger likelihood function value. However, in the reduced χ^2 -values in which the number of parameters are taken into account when determining the goodness of fit, the Λ CDM model has the best value with the Diffusive model Case I (shown in Fig. 1) managing to have a closer value to this accuracy. In order to find the better fitting model among these two cases, we use AIC test, according to which the Diffusive model Cases I and II have obtained more observational and less observational support, respectively. Case I is seen to have a value just missing out on the substantial observational support category, but is still with a closer value to the boundary for less observational support. Therefore, it can be concluded that Case I has some observational support according to the AIC criterion, while Case II has less observational support. In terms of the BIC criteria, we did not obtain one model to have some observational support category, but Case I

was the closer of being in one of the categories. Therefore, statistically, based on the likelihood, the goodness of fit, the AIC and BIC criteria, Case I is the most likely to be an alternative model to the Λ CDM model, with Case II not being ruled out, but will have to be tested on other datasets before being accepted or rejected.

IV. CONCLUSIONS

In this manuscript we considered diffusive cosmological models where dark matter and dark energy interact by exchanging energy. The background cosmological parameters in particular the thermodynamics parameters have been studied and compared against supernova cosmological data for different Diffusive model cases using MCMC simulation results presented in the previous section.

For the two new parameters which arise in our Diffusive cosmological model, namely Δ_m and Δ_Λ , we have examined the Hubble and deceleration parameters results of Figs. 7 to 10 and that of Figs. 17 to 20. Recalling the requirement that the sum of these two parameters need to be zero, the magnitude of Δ_m and Δ_Λ of ≈ 0.0025 fit the parameter space very well. Following which we investigated this deeply based on the statistical analysis made in the above section which is given in Table I. From our analysis we observed that cases having positive values of Δ_m were showing the largest values of likelihood function. Based on the analysis of likelihood, goodness of fit, AIC and BIC criteria, one can conclude that overall Case I is the most likely to be an alternative to the Λ CDM model.

As we have highlighted in the discussion part our current work is to provide a viability test of the different cases considered, but to reject or accept any of them more data and rigorous testing method is needed. Moreover, our initial result such as the one shown in Figs. 7 and 17 suggest that one can look for a potential explanation of the Hubble Tension in such models.

ACKNOWLEDGEMENTS

AA acknowledges that this work is based on the research supported in part by the National Research Foundation (NRF) of South Africa (grant number 112131). This work was part of the research programme “New Insights into Astrophysics and Cosmology with Theoretical Models confronting Observational Data” of the National Institute for Theoretical and Computational Sciences of South Africa.

-
- [1] Adam G Riess, Alexei V Filippenko, Peter Challis, et al. Observational evidence from supernovae for an accelerating universe and a cosmological constant. *The Astronomical Journal*, 116(3):1009, 1998.
 - [2] Saul Perlmutter et al. Supernovae, dark energy, and the accelerating universe. *Physics today*, 56(4):53–62, 2003.

- [3] Subhayan Maity, Pritikana Bhandari, and Subenoy Chakraborty. Universe consisting of diffusive dark fluids: thermodynamics and stability analysis. *The European Physical Journal C*, 79(1):1–8, 2019.
- [4] Max Tegmark, Michael A Strauss, Michael R Blanton, et al. Cosmological parameters from sdss and wmap. *Physical review D*, 69(10):103501, 2004.
- [5] Fritz Zwicky. On the masses of nebulae and of clusters of nebulae. *The Astrophysical Journal*, 86:217, 1937.
- [6] Yoshiaki Sofue and Vera Rubin. Rotation curves of spiral galaxies. *Annual Review of Astronomy and Astrophysics*, 39(1):137–174, 2001.
- [7] Lars Bergström. Dark matter candidates. *New Journal of Physics*, 11(10):105006, 2009.
- [8] Sergio Colafrancesco, S Profumo, and Piero Ullio. Multi-frequency analysis of neutralino dark matter annihilations in the coma cluster. *Astronomy & Astrophysics*, 455(1):21–43, 2006.
- [9] Remudin Reshid Mekuria, Sergio Colafrancesco, Andreas Faltenbacher, and Paolo Marchegiani. Multi-wavelength emissions from dark matter annihilation processes in galaxy clusters using cosmological simulations. *PoS*, HEASA 2016:009, 2017.
- [10] Remudin Reshid Mekuria. *Multi-wavelength emissions from dark matter annihilation processes in galaxy clusters using cosmological simulations*. PhD thesis, University of the Witwatersrand, 2017.
- [11] Mordehai Milgrom. A modification of the newtonian dynamics as a possible alternative to the hidden mass hypothesis. *The Astrophysical Journal*, 270:365–370, 1983.
- [12] Sean M Carroll. The cosmological constant. *Living reviews in relativity*, 4(1):1–56, 2001.
- [13] Steven Weinberg. The cosmological constant problem. *Reviews of modern physics*, 61(1):1, 1989.
- [14] Paul J Steinhardt. A quintessential introduction to dark energy. *Philosophical Transactions of the Royal Society of London. Series A: Mathematical, Physical and Engineering Sciences*, 361(1812):2497–2513, 2003.
- [15] Hermano ES Velten, RF Vom Marttens, and Winifried Zimdahl. Aspects of the cosmological “coincidence problem”. *The European Physical Journal C*, 74(11):1–8, 2014.
- [16] Emmanuel N Saridakis, Ruth Lazkoz, Vincenzo Salzano, et al. *Modified Gravity and Cosmology*. Springer, 2021.
- [17] Salvatore Capozziello and Mariafelicia De Laurentis. Extended theories of gravity. *Physics Reports*, 509(4-5):167–321, 2011.
- [18] Timothy Clifton, Pedro G Ferreira, Antonio Padilla, and Constantinos Skordis. Modified gravity and cosmology. *Physics reports*, 513(1-3):1–189, 2012.

- [19] Ivan Debono and George F Smoot. General relativity and cosmology: unsolved questions and future directions. *Universe*, 2(4):23, 2016.
- [20] Phillip JE Peebles. Evolution of the cosmological constant. *Nature*, 398(6722):25–26, 1999.
- [21] PJE Peebles and Bharat Ratra. Cosmology with a time-variable cosmological ‘constant’. *The Astrophysical Journal*, 325:L17–L20, 1988.
- [22] Martin Reuter and Christof Wetterich. Time evolution of the cosmological “constant”. *Physics Letters B*, 188(1):38–43, 1987.
- [23] Krzysztof Bolejko, Marie-Noëlle Célérier, and Andrzej Krasiński. Inhomogeneous cosmological models: exact solutions and their applications. *Classical and Quantum Gravity*, 28(16):164002, 2011.
- [24] Andrzej Krasinski. *Inhomogeneous cosmological models*. 1997.
- [25] Yuri L Bolotin, Alexander Kostenko, Oleg A Lemets, and Danylo A Yerokhin. Cosmological evolution with interaction between dark energy and dark matter. *International Journal of Modern Physics D*, 24(03):1530007, 2015.
- [26] Weiqiang Yang and Lixin Xu. Cosmological constraints on interacting dark energy with redshift-space distortion after planck data. *Physical Review D*, 89(8):083517, 2014.
- [27] Tao Yang, Zong-Kuan Guo, and Rong-Gen Cai. Reconstructing the interaction between dark energy and dark matter using gaussian processes. *Physical Review D*, 91(12):123533, 2015.
- [28] Winfried Zimdahl. Interacting dark energy and cosmological equations of state. *International Journal of Modern Physics D*, 14(12):2319–2325, 2005.
- [29] MA van der Westhuizen and A Abebe. Dark coupling: cosmological implications of interacting dark energy and dark matter fluids. *Proceedings of the 65th Annual Conference of the South African Institute of Physics (SAIP 2021)*.
- [30] MA van der Westhuizen. Dark interactions beyond the LambdaCDM model. *MSc dissertation*, North-West University, 2022.
- [31] Thabo Mahlatji. Diffusive dark fluids: thermodynamics and cosmological evolution. *Honours research report*, North-West University, 2021.
- [32] Renier Hough, Shambel Sahlu, Heba Sami, Maye Elmardi, Anna-Mia Swart, and Amare Abebe. Confronting the Chaplygin gas with data: background and perturbed cosmic dynamics. *arXiv preprint arXiv:2112.11695*, 2021.
- [33] Nabila Aghanim, Yashar Akrami, Mark Ashdown, et al. Planck 2018 results-vi. cosmological parameters. *Astronomy & Astrophysics*, 641:A6, 2020.